Investigation of the Uptake Rate of Ozone and Methyl Hydroperoxide by Water Surfaces

Laurent Magi, Francis Schweitzer, Cyril Pallares, Sémia Cherif, Philippe Mirabel, and Christian George*

Centre de Géochimie de la Surface/Centre National de la Recherche Scientifique and Université Louis Pasteur, Strasbourg, France

Received: February 21, 1997; In Final Form: April 22, 1997[⊗]

The uptake kinetics of ozone (O_3) and methyl hydroperoxide (CH_3OOH, MHP) by aqueous solutions were studied as a function of temperature using the droplet train technique combined with mass spectrometry detection. The uptake of ozone by pure water was found to be too small to be directly measured. Using NaI as a scavenger increased the uptake coefficient γ from below the detection limit to a range from 0.0037 to 0.0116 for I^- activities in the range from 0.3615 to 2.889 at 282 K. From these experiments, we estimated the second-order rate constant for the reaction $O_3 + I^- \rightarrow$ products to be in the range 3.2×10^8 to 2.4×10^9 M^{-1} s^{-1} for temperature between 275 and 293 K. The activation parameters for this reaction were also estimated. For methyl hydroperoxide, the uptake rate on pure water was fast enough to be directly measured. According to the physicochemical properties of this hydroperoxide, the uptake was mainly due to the diffusion and accommodation processes. It was therefore possible to measure its mass accommodation coefficient α as a function of temperature. The observed values are in the range 0.92×10^{-2} to 2.08×10^{-2} for temperature between 281 and 261 K. The activation parameters for the accommodation were also determined.

Introduction

Ozone plays a central role in the chemistry of the earth's atmosphere. It acts as a shield to solar radiation in the stratosphere (especially for UV radiation) and therefore protects living systems. It is a greenhouse gas and thus participates in atmospheric radiative forcing. It is an important oxidant on its own but is also a precursor for the production of hydroperoxyl (HO_2) radicals and of hydroxyl (OH) radicals, the latter being known as the "atmosphere's detergent".[1] These radicals play a key role in many tropospheric cycles since they control the lifetime of most of the trace gases. For example, in the unpolluted atmosphere, roughly 70% of the OH radical is involved in the oxidation of carbon monoxide (CO) and 30% in the oxidation of methane (CH_4),[2] leading to the formation of methyl hydroperoxide (MHP). Ozone may also react with NO and NO_2 (NO_x) to form higher nitrogen oxides. Recently, numerical simulations by Dentener and Crutzen[3] underlined the importance of heterogeneous reactions for the partitioning of some nitrogen oxides (i.e., N_2O_5 and NO_3) between the gas phase and the liquid phase. They showed that, due to these reactions, the modeled yearly average NO_x burden can decrease by as much as 80%, depending on the season. Since O_3 is correlated to NO_x concentrations, any reduction of nitrogen oxide concentrations will affect ozone and in turn OH concentrations. These heterogeneous processes may then affect the oxidation capacity of the troposphere.

Ozone itself may also be transported to condensed water where it may act as an oxidant, in competition with H_2O_2, for various species such as S(IV), Fe^{2+}, or DMS. Recently, it has been postulated that ozone may also initiate the release of active halogens from sea-salt aerosols that may change the oxidation capacity of the lower troposphere.[4,5] Therefore, it appears that the aqueous phase reactions of ozone may not only represent a significant pathway for its removal from the gas phase but also contribute to changes in the reactivity of tropospheric radicals by changing their absolute levels of concentration in the gas phase as well as the nature of the main oxidant. (Cl may be in competition with OH, for example.)

As already mentioned, the chain oxidation of CH_4 is initiated by ozone, the precursor of OH, leading to formation of different components including methyl hydroperoxide (CH_3OOH, MHP). This hydroperoxide may undergo several processes. In the gas phase, it may react with OH or be photolyzed, which are both processes-generating radicals. An alternative fate is the uptake by clouds or aerosols representing loss or terminating steps. In the aqueous phase, MHP may act as a precursor of radicals through its photodissociation or as a potential oxidant. In fact, it has been shown that its reactivity is similar to that of H_2O_2,[6] and therefore MHP may be involved in the oxidation of S(IV).[7]

To access the role of both species, i.e., ozone and MHP, in the wet chemistry of the atmosphere, one has to consider not only their rate of formation/destruction in the gas phase and the rate at which they react in the aqueous phase but also the rate at which they are transferred to the condensed phase. At the present time, some work is already available for the uptake rate of ozone by an aqueous surface,[8−11] but this parameter is still unknown for MHP. It is therefore the aim of this article to determine uptake rates for MHP on aqueous surfaces as a function of temperature. In addition, we have also studied uptake rates for ozone as a function of temperature.

Heterogeneous Gas/Liquid Kinetics

The rate of uptake of a trace gas by a liquid is a multistep process that can be related to fundamental properties of the gas, interface, and the condensed phase such as mass accommodation coefficient, solubility, and reactivity.

The uptake process can be summarized as follows: (1) diffusion of the molecules in the gas phase toward the liquid interface, (2) transfer across the interface (accommodation process), (3) diffusion and reaction in the condensed phase, and (4) eventually, diffusion out and desorption of the reaction products.

The rate at which a trace gas molecule may be transferred, from a well-mixed gas phase at a given concentration n_{mixed},

* Corresponding author. e-mail: george@illite.u-strasbg.fr.
[⊗] Abstract published in *Advance ACS Abstracts,* June 1, 1997.

S1089-5647(97)00646-9 CCC: $14.00

into the condensed phase can be obtained from the kinetic theory of gases. This allows the calculation of the maximum flux Φ_{max} that may cross the interface

$$\Phi_{max} = {}^1/_4\langle c\rangle n_{mixed}\alpha \quad (1)$$

where $\langle c\rangle$ is the trace gas average thermal velocity and α is the mass accommodation coefficient that characterizes the gas/liquid efficiency for the accommodation process. It represents the probability that a molecule, impinging on the interface, will be transferred into the condensed phase. The effective flux Φ_{eff} actually crossing the interface may be lower than that given by eq 1 for several reasons. If the uptake is very efficient, then concentration profiles in the gas phase may build up due to a slow diffusion process. In such a case, the concentration of the trace gas molecules nearby the interface will be lower compared to the well-mixed situation, meaning that Φ_{eff} is lower than Φ_{mixed}. Another possibility that may limit the uptake rate is introduced by solubility effects. If the trace gas solubility is very low, then a desorption flux may build up with time, due to the saturation of the interface. In this situation, the effective flux Φ_{eff} is given by the difference of the in- and out-going fluxes. At equilibrium, both in- and out-coming fluxes are equal in intensity, and no effective flux is observed. Finally, if the reactivity of the dissolved species is very low, the effective rate of mass transfer may be limited by the rate at which it is transformed in the condensed phase.

If the flux is limited by one or more of the processes mentioned above, eq 1 is no longer valid. To overcome this difficulty, one may consider the following definition of the effective flux crossing the interface

$$\Phi_{eff} = {}^1/_4\langle c\rangle n_{mixed}\gamma \quad (2)$$

which is very similar to eq 1, but where α has been replaced by the uptake coefficient γ. This parameter can be defined as the probability that a striking molecule will be taken up by the condensed phase (similarly to α) but considering now the overall uptake process. Therefore, the uptake coefficient γ will be a function of the diffusion rates in both phases (described by the respective diffusion coefficients), of the accommodation process (described by the accommodation coefficient α), of the solubility (which depends upon the Henry's law constant), and of the reactivity in the liquid phase (controlled by the rate constant). To each of these processes, one can attribute a specific uptake coefficient according to[12]

$$\text{diffusion limitation: } \frac{1}{\gamma_{diff}} = \frac{\langle c\rangle d_{eff}}{8D_g} - \frac{1}{2} \quad (3)$$

$$\text{saturation limitation: } \gamma_{sat} = \frac{8HRT\sqrt{D_a}}{\langle c\rangle\sqrt{\pi t}} \quad (4)$$

$$\text{reactivity limitation: } \gamma_{rxn} = \frac{4HRT\sqrt{kD_a}}{\langle c\rangle} \quad (5)$$

where d_{eff} is the effective droplet diameter,[13] H is the Henry's law constant, R is the perfect gas constant, T is the temperature, D_g and D_a are the gas and aqueous phase diffusion coefficients, t is the gas/liquid contact time, and k is the first-order rate constant for a given reaction in the liquid phase. The overall uptake coefficient can be calculated by summing the individual resistance (defined as the inverse of the specific uptake coefficient) according to[14]

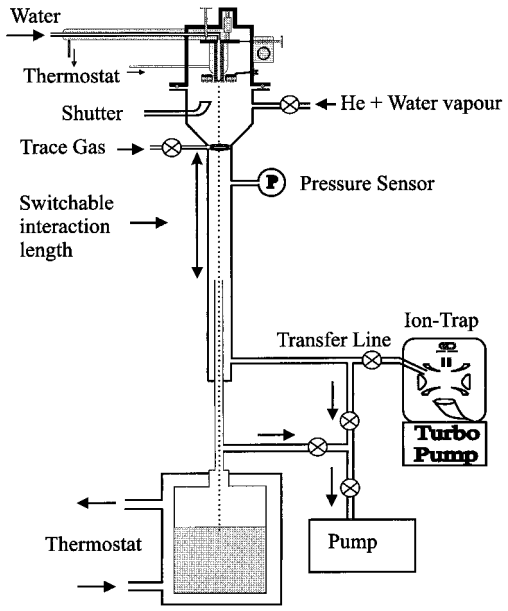

Figure 1. Schematic representation of the newly constructed droplet train setup.

$$\frac{1}{\gamma} = \frac{1}{\gamma_{diff}} + \frac{1}{\alpha} + \frac{1}{\gamma_{sat} + \gamma_{rxn}}$$

$$= \frac{\langle c\rangle d_{eff}}{8D_g} - \frac{1}{2} + \frac{1}{\alpha} + \frac{\langle c\rangle}{4HRT\sqrt{D_a}}\left(\frac{2}{\sqrt{\pi t}} + \sqrt{k}\right)^{-1} \quad (6)$$

This relation clearly shows that the uptake coefficient is a function of different fundamental properties of the molecule such as solubility, diffusion, etc. The treatment used to obtain eq 6 is very similar to the one used for the calculation of deposition velocity on the ocean surface.[15]

Experimental Section

Apparatus. The newly constructed droplet train apparatus depicted in Figure 1 involves a highly controlled droplet train passing through different zones at low pressure (typically between 10 and 30 Torr). These latter are the droplet generation area, a droplet conditioning zone, the interaction chamber where the trace gas can react with the train of droplets, and finally the collection chamber where the aqueous phase is collected. By measuring the change of trace gas density after the gas/liquid interactions, it becomes possible to determine the kinetics of the different processes involved.

One of the major difficulties in studying gas/liquid interactions is to obtain a very well-defined liquid surface that can be rapidly renewed. To overcome this difficulty, we use a train of high-speed droplets generated by the vibrating orifice method, based on forcing water through a calibrated orifice that is excited by a piezoelectric ceramic. Then its vibration controls the disintegration of the jet emerging from the orifice, leading to a very well-defined liquid surface. In this study, the water was forced through a calibrated orifice (75 μm diameter) by a typical 2−4 bar back-pressure leading to droplet diameters in the range 80−150 μm. The exact diameters were determined from the vibration frequency f of the orifice (4−50 kHz) and the liquid volume flow rate (F_l), in the range 1.5−5 mL min^{-1}, using

$$d = (6F_l/\pi f)^{1/3} \quad (7)$$

Since the jet passes through the orifice and disintegrates with negligible energy losses, the speed of the droplets can be

calculated from the liquid flow rate and the orifice's surface. In this study, these velocities were in the range 1500−2000 cm s^{-1}, leading to short transit times of the droplets in the interaction chamber (i.e., 2−20 ms). The quality of the droplet train is monitored in the interaction chamber using a diode coupled with the frequency generator. The validity of eq 7 was checked experimentally using laser scattering.[16] The agreement between theory and experimental data was generally better than 3%.

The interaction chamber is a vertically aligned flow tube with a 1.8 cm i.d. Its length can be varied up to 20 cm, in order to change the gas/liquid interaction time or the surface exposed by the droplet train. This surface can also be changed by switching, during an experiment, the frequency of production of the droplets, affecting more the droplets number than their size which varies as $f^{1/3}$. Since the uptake process is directly related to the surface S exposed by the droplets, any change ΔS in this surface results in changes Δn of the trace gas density at the exit ports of the flow tube. In fact, by considering the kinetic gas theory, it becomes possible to calculate the instantaneous uptake rate as

$$\frac{dn}{dt} = -\Phi_{eff}\frac{S}{V} \tag{8}$$

$$\frac{dn}{dt} = -\frac{S}{V}\frac{\langle c\rangle}{4}\gamma_{obs}n \tag{9}$$

where S is the total surface exposed by the droplet train, γ_{obs} is the experimental uptake coefficient, and V is the volume of the interaction chamber. However, since we are measuring the averaged signal during the transit time due to changes in the exposed surface**,** we have to integrate eq 9, leading to[13]

$$\gamma_{obs} = \frac{4F_g}{\langle c\rangle \Delta S}\ln\left(\frac{n}{n-\Delta n}\right) \tag{10}$$

where F_g is the carrier gas volume flow rate and n is the trace gas density before frequency or length switching. Typical experimental values for F_g are in the range 200−650 mL min^{-1} STP. By measuring the fractional changes in concentration ($n/n - \Delta n$) as a function of $4Fg/(\langle c\rangle \Delta S)$, it becomes possible to determine the overall uptake coefficient γ_{obs}. This parameter can be measured as a function of the total pressure, gas/liquid contact time, or composition of the liquid used to produce the droplets. These last measurements are necessary to decouple the overall process into individual steps.

An important aspect of this technique is the careful control of the partial pressure of water in the flow tube since it controls the surface temperature of the droplets through evaporative cooling.[13] Therefore, the carrier gas (helium) was always saturated, at a given temperature, with water vapor before entering the flow tube. The equilibrium between ambient saturated helium and the liquid droplets is reached in the first zone of the setup before the interaction zone. The liquid used to produce the droplets was thermostated up the orifice, for temperatures higher than 0 °C, leading to fast equilibrium attainment. Temperatures lower than 0 °C were obtained through evaporative cooling of the droplets in the first part of the flow tube. At these lower temperatures, the droplets are supercooled but not frozen, even for temperatures lower than −20 °C.[13] However, for supercooled droplets the temperature refers to the surface thermal equilibration, which occurs on a time scale of about 1 ms and is therefore obtained before the droplets reach the region where they are exposed to the trace gases. Thermal conduction for our droplets has a characteristic time of about 10 ms, meaning that although the surface quickly equilibrates with the ambient water vapor, the interior of the droplets' volume will not be at equilibrium. As shown by Worsnop et al.,[13] the measured uptake rate is therefore an average over a range up to 3 K around the desired temperature (including an uncertainty of 10% on the water partial pressure).

Gas Production and Analytical Methods. Ozone was produced by an electrical discharge generator (Sorbios Model GSG 001.2) from a very small flow of pure O_2 (Prodair, 99.95%) and was directly injected into the flow tube of the droplet train apparatus after dilution in helium (99.999%) using calibrated mass-flow controllers.

Methyl hydroperoxide (MHP) was prepared according to the standard method described by Rieche and Hitz.[17] However, MHP was never isolated but was purified by extraction with diethyl ether and concentrated by boiling off the excess ether. By employing this method, we do avoid the hazardous distillation of this hydroperoxide.[18] Diethyl ether was nearly always present as an impurity but did not interfere with the uptake measurements.

Aqueous solutions used to prepare the droplets were prepared from Milli-Q water (18 MΩ cm) and reagent grade sodium iodide (Prolabo) when necessary (see below).

An ion trap detector (Varian Model Saturn 4D) was connected to the exit ports of the flow tube in order to monitor the gas phase concentration of MHP and O_3. This setup is equipped with electron impact and chemical ionization, but only the first technology was used in the present study. A small flow of gas (∼1 mL min^{-1}) was injected into the trap and ionized with an electron beam (70 eV), and the resulting signal was integrated over 1 s and recorded. However, due to the high pressure in the trap (∼10^{-3} Torr), fragmentation processes are important, and we were not able to detect the molecular peak of ozone at m/e 48. Therefore, we titrated O_3 with NO (Alphagaz) before entering the ion trap, and we followed the signal generated by NO_2 at m/e 46 (NO_2) as an indicator for O_3 concentrations. For MHP, we were able to obtain mass spectra in good agreement with literature data,[19] obtained at 20 eV, where it was found that the peak at m/e 48 (M) and 47 (M − 1) have nearly the same intensity as shown in Figure 2. FTIR spectroscopy was also employed in order to identify the methyl hydroperoxide. The system used consisted of a Nicolet Protégé 460 spectrometer equipped with an IRA long path White cell (light path in the range from 2.2 to 22 m) with KBr windows. Infrared spectra were taken in the range from 4000 to 400 cm^{-1} and were coadded in order to increase the signal-to-noise ratio. Again, obtained spectra (Figure 2) are in good agreement with literature data.[20]

Results and Discussion

Ozone. The uptake of ozone in pure water, due to its the physical solubility, can be estimated from eq 6 and from its bulk properties. Using the Henry's law constant H given by Chameides,[21] i.e., $H = 1.15 \times 10^{-2}$ M atm^{-1} at 298 K and the aqueous phase diffusion coefficient, $D_a = 1.85 \times 10^{-5}$ cm^2 s^{-1} at 298 K, measured by Matrozov et al.,[22] the uptake rate of ozone on pure water is found to be very low, i.e., $\gamma \approx 3 \times 10^{-6}$ at 298 K and 5 ms contact time. (Note that the value of D_a, with a T/η temperature dependence, where η is the water viscosity,[23,24] was used throughout this work even for NaI solutions.) Such a low uptake is far beyond the limit of sensibility of our apparatus, i.e., 10^{-3} with the present gas phase analysis or 10^{-5} with aqueous phase detection[16] which was not used here. Therefore, we had to add a scavenger (NaI) to the solution in order to enhance the uptake rate of ozone, enabling the determination of its reactivity toward iodide as a function of temperature.

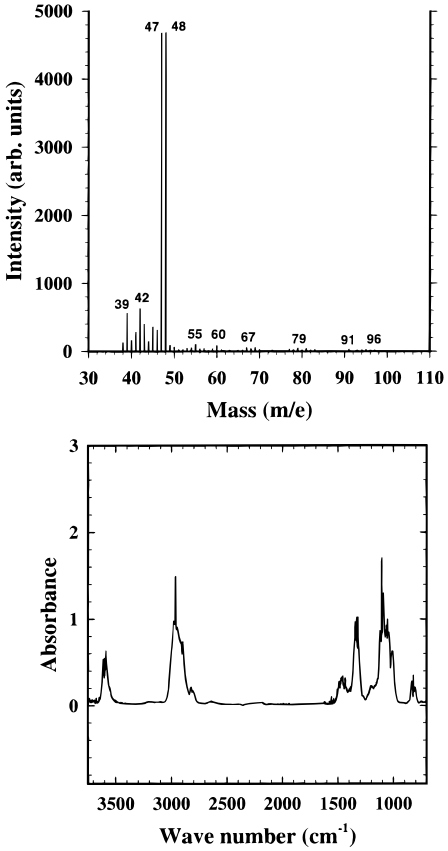

Figure 2. Typical mass (upper part) and infrared (lower part) spectra of the methyl hydroperoxide. Both of them are in good agreement in literature reference spectra (see text). No important impurity affects our identification. The peak at *m/e* 48 was used for the kinetics measurement.

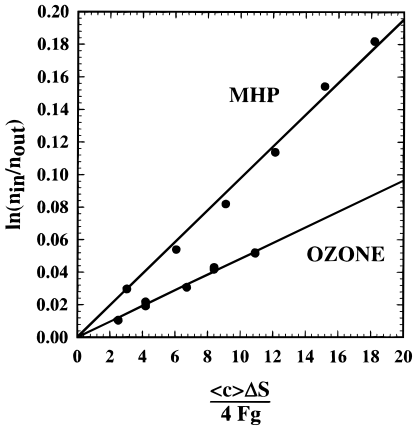

Figure 3. Typical plots of $\ln(n_{in}/n_{out})$ versus $\langle c\rangle \Delta S/4Fg$ for O_3 on a 1 M NaI ($a_{I^-} = 0.736$) and CH_3OOH on pure water at 281 K according to eq 10. The slopes of such plots are a measure of the uptake coefficient γ. The solid represents a linear fit to our data.

Figure 3 shows an example of data obtained, at 281 K, for the uptake of ozone plotted according to eq 10. (Similar plots were also obtained at the other temperatures, i.e., 275, 288, and 293 K.) The individual slopes of such lines yield the values of the uptake coefficients γ_{obs}, and as can be seen from this figure, the excellent linearity validates the measurement procedure. In addition, the influence of several factors has been studied, i.e., the influence of NaI concentration and of the temperature. Figure 4 depicts the dependence, at 281 K, of the uptake coefficient on the scavenger concentration (which varied from 0.5 to 3 M) and more precisely on the activity a_I- of I^-. Activities had to be used because of the relatively high

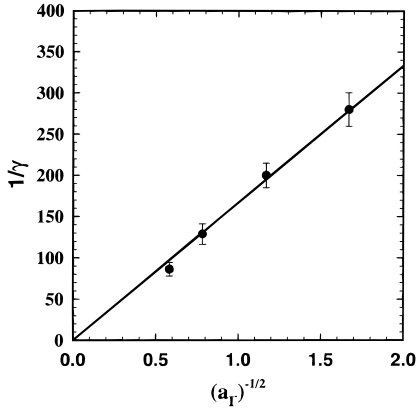

Figure 4. Plot of $1/\gamma$ versus a_{I^-} at 281 K according to eq 11. The solid line represents a linear fit to our data. The slope of such a fit yield value of $H\sqrt{k}$. The error bars are given at the 2σ level.

concentrations of NaI in the solutions employed in order to enable the measurement of the uptake kinetics. At 281 K, for activities ranging from 0.36 to 2.89 (i.e., concentrations from 0.5 to 3 M), the measured uptake coefficients were in the range 3.7×10^{-3} to 11.6×10^{-3}, i.e., highly dependent on the NaI content. Figure 4 also shows a plot of $1/\gamma_{obs}$ versus $1/a_{I^-}^{1/2}$ according to the following eq[13]

$$\frac{1}{\gamma_{obs}} = \frac{1}{\gamma_{diff}} + \frac{1}{\alpha} + \frac{\langle c\rangle}{4HRT\sqrt{k^I D_a}} \qquad (11)$$

where k^I is the pseudo-first-order rate constant for the reaction $O_3 + I^- \rightarrow$ products ($k^I = k^{II}a_I-$). Equation 11 is a simplified version of the more complete description (eq 6) where γ_{sat} has been omitted due to its very low value compared to γ_{rxn}. This simplification simply means that, in the presence of NaI, the uptake of ozone is not limited by its solubility but more realistically by its chemical rate of transformation in the bulk.

According to eq 11, the intercept in Figure 4 contains information on $(1/\gamma_{diff} + 1/\alpha)$. However, as it can be seen from this figure, the intercept is very small, i.e., our measured kinetics does not enable any direct measurement of α since our intercepts are spread around the origin. Therefore, a precise value for α cannot be given, and we can only provide a lower limit of about 10^{-1}. If the uptake is limited by the reactive loss of O_3 in the bulk, i.e., if $1/\gamma_{obs} \gg (1/\gamma_{diff} + 1/\alpha)$, then γ_{obs} is directly proportional to $H\sqrt{k^I D_a}$ (i.e., the first two terms of the right-hand side of eq 11 can be omitted), allowing the determination of the rate constants k^I and k^{II} for the reaction between iodide and ozone, provided that H and D_a are known. Using for H and D_a the values previously mentioned, the values obtained for k^{II} are shown, as a function of temperature, in Figure 5. They range from $(3.2 \pm 1.5) \times 10^8$ M^{-1} s^{-1} at 275 K to $(2.4 \pm 1.3) \times 10^9$ M^{-1} s^{-1} at 293 K. The corresponding activation parameters obtained from an Arrhenius plot (Figure 5) are $A = 1.4 \times 10^{22}$ M^{-1} s^{-1} and $E_a = 73.08$ kJ, with an estimated error of 40%. Activation energies of comparable magnitudes have already been reported for the reaction of ozone and H_2O_2.[25]

All the results, obtained in the above section, have been calculated by ignoring the possible variation of the Henry's law constant H, with the ionic strength (salting effect) and the pH. Such variations are known to occur, and since we were working with relatively high concentrations of salt (up to 3 M), we shall know examine their effects. The variation of H with the concentration of salt, or more precisely with the ionic strength I, is given by

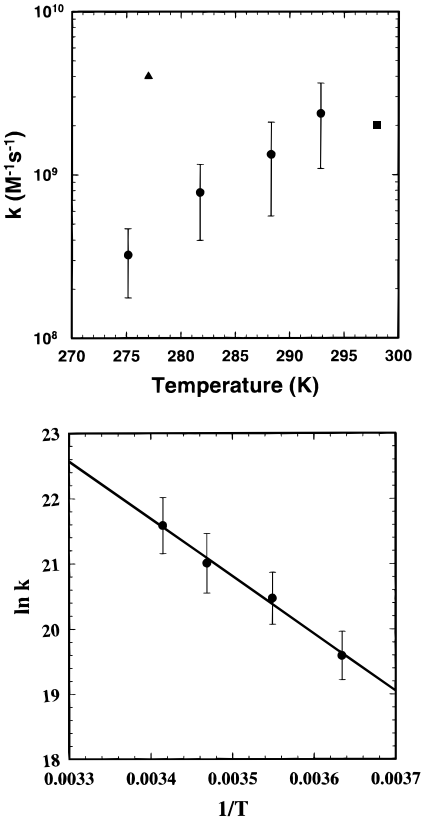

Figure 5. Rate constant, for the reaction $O_3 + I^- \rightarrow$ products as a function of temperature (upper part) (triangle, Hu et al.;[11] square: Garland et al.;[28] circle, this work) and Arrhenius plot (lower part). The error bars are given at the 2σ level.

TABLE 1: Setchenow Coefficients, as a Function of Temperature, for O_3 in NaI Solutions[a]

T (K)	h_{Na^+} (M^{-1})	h_{I^-} (M^{-1})	h_{O_3} (M^{-1})
276	0.091	0.005	−0.0424
282	0.091	0.005	−0.0191
288	0.091	0.005	0.00501
293	0.091	0.005	0.0211

[a] h_{Na^+} and h_{I^-} have been taken from Danckwerts[26] whereas h_{O_3} has been derived from Kosak-Channing and Helz.[27]

$$\log(H/H_{salt}) = hI \qquad (12)$$

where H_{salt} is the Henry's law constant for a NaI solution and h is the Setchenow coefficient for this system. This coefficient can be expressed as a sum of the individual contributions due to the nature of the ions and of the dissolving gas:[26] $h = h_{Na^+} + h_I- + h_{O_3}$. The values of h_{Na^+} and h_I-, independent of temperature, have already been determined, but not that of h_{O_3}. However, using the results of Kosak-Channing and Helz,[27] who studied the solubility of ozone in aqueous solutions of Na_2SO_4, it was possible to extract information on the Setchenow coefficient h_{O_3} for O_3 as a function of temperature (see Table 1). This allowed recalculation of the Henry's law constant H_{salt} for a NaI solution as a function of the ionic strength (Table 2). Considering that the slope in Figure 4 is constant, $H\sqrt{k}$ is also constant and one can calculate the effect of the presence of salt on the rate constant (Table 2) using H_{salt} calculated with eq 12. The salting effect on the aqueous phase diffusion coefficient is smaller than 12%, as estimated from the changes in viscosity when changing from pure water to 3 M NaI. Since only the square root of D_a is needed in eq 11, the uncertainty arising from this effect is less than 6% and has been neglected. As can be seen from Table 2, there is a general tendency for k_{salt} to increase with the ionic strength of the solution, but the variations remain within the error limits of our determinations. The best estimate that we can provide for k are then obtained directly from eq 11, where such effects have been omitted. They are given in Table 2 as k^0.

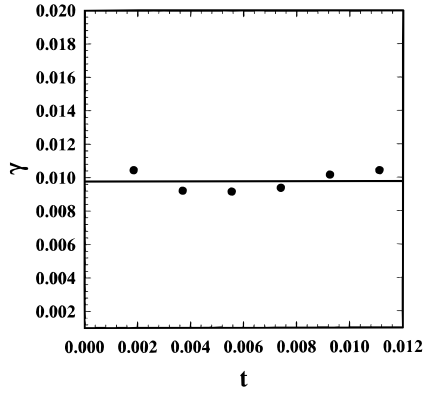

Figure 6. Uptake of methyl hydroperoxide as a function of gas/liquid interaction time at 281 K. Within the experimental scattering no lowering of the uptake coefficient γ is visible, meaning that surface saturation effects are beyond the sensitivity of this technique.

Comparison with Previous Results. Utter et al.,[8] using a wetted wall flow tube and different scavengers (Na_2SO_3, $Na_2S_2O_3$, and $SnCl_2$), reported a lower limit of $2\ 10^{-3}$ at 276 K for the mass accommodation coefficient. However, no definite value was given since the different scavengers used lead to inconsistent results. And these authors concluded that α should be close to one. Tang and Lee[10] using a bulk surface reported a value of 5×10^{-4}, which may considered as a lower limit because of the influence of sulfite used as a scavenger. (See for example the discussion in ref 8.) More recently, Wunderlich et al.,[9] using the liquid jet technique at room temperature and KI as a scavenger, reported a value of 5×10^{-3}. However, as quoted in a later work,[28] they used a value of $10^6\ M^{-1}\ s^{-1}$ for k^{II} in their numerical modeling of the uptake. If the value of k^{II} reported here is used, then their previous numerical simulation overestimated the iodide concentration at the jet's surface and therefore underestimated the value of α. Finally, our lower limit of 0.1 for α is comparable with the value of 0.1 reported by Hu et al.,[11] who used the same experimental procedure.

Concerning the estimated reaction rate constants, our determination, i.e., $2.4 \times 10^9\ M^{-1}\ s^{-1}$ at 293 K, closely agrees with the values obtained by Garland et al.,[29] i.e., $2 \times 10^9\ M^{-1}\ s^{-1}$ at 298 K. At lower temperatures, Hu et al.[11] deduced from their work a value of $4 \times 10^9\ M^{-1}\ s^{-1}$ at 277 K, which is larger than those reported for 293−298 K and which agrees with our value (3.2×10^8 at 276 K) only by 1 order of magnitude.

Methyl Hydroperoxide. In Figure 3, we also plotted typical raw data for MHP according to eq 10. Again, the value of γ is extracted from the slope of this plot. For this hydroperoxide, and contrary to ozone, it was possible to measure directly the uptake kinetics without adding any scavenger since the solubility is much higher. In addition, MHP hydrolysis is known to be very slow,[31] and as a consequence, γ_{rxn} may be neglected in eq 6. Furthermore, the study of the uptake kinetics of MHP as a function of gas/liquid contact time (and temperature) shows that the uptake coefficient γ is time independent, within the experimental errors (Figure 6). This means that no saturation effect is visible in the temperature range studied here (261−281 K), i.e., that the Henry's law constant H is large enough so that γ_{sat} is negligibly small compared to γ. A lower estimate of H can be calculated by considering that, in Figure 6, a time dependence of γ leading to a variation of 10% in the slope would be observable. Such a variation would correspond to a Henry's law constant of about 700 M atm^{-1}, value which has to be

TABLE 2: Kinetics of the Reaction of $O_3 + I^-$ as a Function of Ionic Strength Derived from the Salting-Out Effect Estimated according the Setchenow Equation[a]

ionic strength (M)	$10^3\gamma$	$Hk^{1/2}$ (M atm^{-1} s$^{-1/2}$)	H^0 (M atm^{-1})	H_{salt} (M atm^{-1})	k^0 (s^{-1})	k_{salt} (s^{-1})
276 K						
0.5	2.6 ± 0.2	433.1	0.0245	0.0239	3.2×10^8	3.3×10^8
1	4.1 ± 0.3	479.8	0.0245	0.0232	3.2×10^8	4.3×10^8
2	5.1 ± 0.5	403.3	0.0245	0.0220	3.2×10^8	3.6×10^8
3	6.9 ± 0.7	405.2	0.0245	0.0209	3.2×10^8	3.8×10^8
282 K						
0.5	3.57 ± 0.3	545.7	0.0197	0.0190	7.8×10^8	8.3×10^8
1	5.0 ± 0.4	534.8	0.0197	0.0182	7.8×10^8	8.6×10^8
2	7.8 ± 0.7	558.1	0.0197	0.0169	7.8×10^8	1.1×10^9
3	11.6 ± 0.6	625.8	0.0197	0.0156	7.8×10^8	1.6×10^9
288 K						
0.5	3.8 ± 0.3	541.2	0.0160	0.0152	1.3×10^9	1.4×10^9
1	6.9 ± 0.9	677.1	0.0160	0.0145	1.3×10^9	2.2×10^9
2	8.4 ± 0.7	556.4	0.0160	0.0131	1.3×10^9	1.8×10^9
3	13.3 ± 0.7	662.9	0.0160	0.0118	1.3×10^9	3.1×10^9
293 K						
0.5	5.0 ± 0.5	668.9	0.0140	0.0132	2.4×10^9	2.6×10^9
1	8.1 ± 0.8	760.2	0.0140	0.0125	2.4×10^9	3.7×10^9
2	9.6 ± 0.9	610.6	0.0140	0.0111	2.4×10^9	3.1×10^9
3	13.5 ± 0.7	644.4	0.0140	0.0099	2.4×10^9	4.3×10^9

[a] $Hk^{1/2}$ is calculated directly from eq 11 where only the last term of the right-hand side has been considered (this is justified by the zero intercept in Figure 4) and from the measured values of γ; H^0 is the Henry's law constant in pure water (taken from ref 21), and k^0 is the second-order rate constant determined from the values of $Hk^{1/2}$; H_{salt} is the Henry's law constant affected by salt effects (calculated using H^0 and eq 12), and k_{salt} is the corresponding rate constant determined from $Hk^{1/2}$ measurements.

considered as a lower limit. This lower limit is in good agreement with the Henry's law constant measured by Lind and Kok[7] and O'Sullivan et al.,[31] i.e., 960 and 970 M atm^{-1}, respectively. These values are larger than our estimate, giving support to the time independence of γ. Therefore, eq 6 can be simplified to

$$\frac{1}{\gamma} = \frac{\langle c \rangle d_{eff}}{8D_g} - \frac{1}{2} + \frac{1}{\alpha} \qquad (13)$$

In eq 13, $d_{eff} = 1.8 d_{orifice}$ and $d_{orifice}$ is the diameter of the calibrated orifice used to produce the droplets.[13] D_g, the diffusion coefficient of MHP in helium, was estimated from the value of D_g for ethanol after correction for the mass difference.[32]

The mass accommodation coefficient α can be extracted from γ after correction for gas phase diffusion limitations (eq 13). However, as already noted, the use of this equation implies that MHP only reacts slowly with water, which is effectively the case.[31] We must also note that, in regard to the high solubility of MHP at the temperatures used here, it is extremely difficult to obtain reliable information on the liquid phase processes (i.e., reactivity in the aqueous phase). In some experiments, we wetted the wall of the flow tube with stagnant water and observed an extremely small increase of the signal at *m*/*e* 30, which was attributed to the formation of gas phase formaldehyde (H_2CO). It was not possible to quantify the kinetics of this reaction because it was much too slow to be studied with the techniques presently available in our group. Therefore, it appears that the uptake of MHP can be regarded as nonreactive, within the experimental time scale of the droplet train technique.

Figure 7 shows the calculated values of α as a function of temperature. The plot exhibits a negative temperature dependence, in agreement with what has been previously observed by Jayne et al.[33] for highly soluble gases for which the rate-limiting step is a part of the physical solvation process. In the model developed by Davidovits et al.,[34] their mass accommodation coefficient can be expressed as

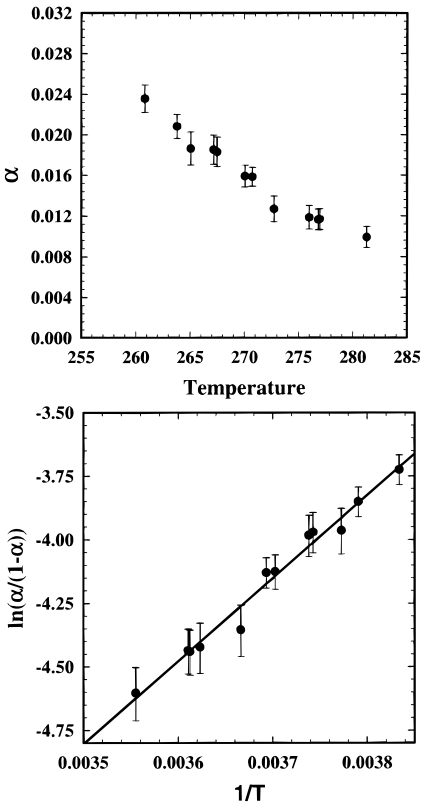

Figure 7. Mass accommodation of methyl hydroperoxide as a function of temperature (upper part) and a representation of $\ln(\alpha/1-\alpha)$ versus $1/T$ according to eq 13. The solid line represents a linear fit to our data and its results given values of $\Delta H^{\ddagger}_{obs}$ and $\Delta S^{\ddagger}_{obs}$. The error bars are given at the 2σ level.

$$\ln\left\{\frac{\alpha}{1-\alpha}\right\} = -\frac{\Delta G^{\ddagger}_{obs}}{RT} \qquad (14)$$

where $\Delta G^{\ddagger}_{obs}$ can be regarded as the height of the Gibbs free energy barrier for the transition between the gas and solvated state. The enthalpy ΔH_{obs} and entropy ΔS_{obs} can be derived from a plot of $\ln(\alpha/(1-\alpha))$ versus $1/T$ as displayed in Figure

7. The slope of such a plot corresponds to $-\Delta H_{obs}/R$ while the intercept corresponds to $\Delta S_{obs}/R$. The values obtained for ΔS_{obs} and ΔH_{obs} are -32.5 ± 2.2 cal mol^{-1} K^{-1} and -6.5 ± 0.6 kcal mol^{-1} K, respectively, where the specified error represents 2 standard deviations.

In order to explain the generally observed negative temperature dependence of α, Davidovits et al.[34] developed a model, later modified by Nathanson et al.[35] in order to improve the description of the dynamics at the interface, in which mass accommodation is depicted as a continuous nucleation process where only clusters reaching a critical size (defined as N^*) by condensation are taken up by the nearby liquid phase. The critical size is defined as the number of molecules in the cluster or more precisely the number of hydrogen bonds used to form the cluster. In this theory, there is a direct relationship between ΔH_{obs} and ΔS_{obs} governed by N^*. Our measured values are found to agree with this formulation with a critical size $N^* \sim 2$. It is interesting to note that the values of ΔH_{obs} and ΔS_{obs} found for CH_3OOH are between those reported for methanol ($\Delta H_{obs} = -8.0$ kcal mol^{-1} and $\Delta S_{obs} = -34.9$ cal mol^{-1} K^{-1}) and for hydrogen peroxide[35] ($\Delta H_{obs} = -5.5$ kcal mol^{-1} and $\Delta S_{obs} = -22.5$ cal mol^{-1} K^{-1}). However, the values for CH_3OOH, are closer to those for CH_3OH indicating that the rate-limiting step in the accommodation process is similar for both compounds. In such a situation, there is predominantly only one hydrogen-bonding site in the hydroperoxy group compared to the presence of two sites in H_2O_2. Such an observation can probably be extended to other hydroperoxides in order to estimate their accommodation coefficients for atmospheric modeling studies.

Conclusion

In the real atmosphere as well as in our laboratory study, the uptake of ozone will be governed by its reactivity toward dissolved species. The concentrations of iodide used here are definitively orders of magnitude larger than those encountered in actual liquid aerosols. Therefore, the reaction between ozone and I^- may not be relevant for atmospheric liquid aerosol chemistry. However, as shown by Garland et al.,[28] with a rate constant on the order of 10^9 M^{-1} s^{-1}, 20% of ozone absorbed by sea water may react with dissolved iodide, producing molecular iodine that may partly be rejected to the gas phase where it may form active iodide radicals. These latter radicals are actually expected to react with ozone, explaining the observed upper troposphere ozone profiles. However, this source is probably minor compared to other ones.

The measured uptake kinetics for methyl hydroperoxide agree well with measured Henry's law constant and allowed the first determination of its mass accommodation coefficient as a function of temperature. The order of magnitude of this parameter falls in the range where interfacial mass transport limitation may occur.[36] Therefore, these measurements may be of importance for modeling studies where phase transfer of this hydroperoxide has to be included.

Acknowledgment. Supported of this work by the European Commission (Project RINOXA, EV5V-CT93-0317) is gratefully acknowledged.

References and Notes

(1) Graedel, T. E.; Crutzen, P. J. *Atmospheric Change—An Earth System Perspective*; W. H. Freeman: New York, 1993.

(2) Wayne, R. P. *Chemistry of Atmospheres;* 2nd ed.; Clarandon Press: Oxford, 1991.

(3) Dentener, F. J.; Crutzen, J. *J. Geophys. Res*. **1993**, *98*, 7149.

(4) Behnke, W.; Elend, M.; Krüger, H. U.; Scheer, V.; Zetzsch, C. In *Transport and Transformation of Pollutants in the Troposphere, Proceedings of EUROTRAC Symposium '96*; Borrell, P. M., Borrell, P., Cvitas, T., Kelly, K., Seiler, W., Eds.; Computational Mechanics Publications: Southampton, 1996; Vol. 1, pp 463−468.

(5) Vogt, R.; Crutzen, J. C. *Nature* **1996**, *383*, 327.

(6) Warneck, P. In *Heterogeneous and Liquid-Phase Processes;* Warneck, P., Ed.; Springer-Verlag: Berlin, 1996; Eurotrac Vol. 2.

(7) Lind, J. A.; Kok, G. L. *J. Geophys. Res*. **1986**, *91*, 7889.

(8) Utter, R. G.; Burkholder, J. B.; Howard, C. J.; Ravishankara, A. R. *J. Phys. Chem*. **1992**, *96*, 4973.

(9) Wunderlich, C.; Schlemm, A.; Hesse, K.; Hupperich, D.; Schurath, U. In *Tropospheric Oxidation Mechanisms*; Air Pollut. Res. Rep. 54; Becker, K. H., Ed., Comm. of the Eur. Communities: Brussel, 1994; Report EUR 16171 EN, pp 45−50.

(10) Tang, I. N.; Lee, J. H. *The Chemistry of Acid Rains; Sources and Atmospheric Processes*; Johnson, R. W., Gordon, G. E., Eds.; ACS Symposium Series 349; American Chemical Society: Washington, DC, 1987; pp 109−117.

(11) Hu, J. H.; Shi, Q.; Davidovits, P.; Worsnop, D. R.; Zahniser, M. S.; Kolb, C. E. *J. Phys. Chem*. **1995**, *95*, 8768.

(12) Kolb, C. E.; Worsnop, D. R.; Zahniser, M. S.; Davidovits, P.; Hanson, D. R.; Ravishankara, A. R.; Keyser, L. F.; Leu, M. T.; Williams, L. R.; Molina, M. J.; Tolbert, M. A. Laboratory Studies of Atmospheric Heterogeneous Chemistry; Current Problems in Atmospheric Chemistry. In *Advances Series in Physical Chemistry*; Ng, C.-Y., Ed.; World Scientific: Singapore, 1995; Vol. 3, pp 771−875.

(13) Worsnop, D. R.; Zahniser, M. S.; Kolb, C. E.; Gardner, J. A.; Watson, L. R.; Van Doren, J. M.; Jayne, J. T.; Davidovits, P. *J. Phys. Chem*. **1989**, *93*, 1159−1172.

(14) Jayne, J. T.; Duan, S. X.; Davidovits, P.; Worsnop, D. R.; Zahniser, M. S.; Kolb, C. E. *J. Phys. Chem*. **1992**, *96*, 5452.

(15) Liss, P. S.; Slater, P. G. *Nature* **1974**, *247*, 181.

(16) Ponche, J. L.; George, Ch.; Mirabel, Ph. *J. Atmos. Chem*. **1993**, *16*, 1.

(17) Rieche, A.; Hitz, F. *Ber. Dtsch. Chem. Ges. B* **1929**, *62*, 2458.

(18) Vahjiani, G. L.; Ravishankara, A. R. *J. Phys. Chem*. **1989**, *93*, 1948.

(19) Heicklen, J.; Johnston, H. S. *J. Am. Chem. Soc*. **1962**, *84*, 4030.

(20) Barnes, I.; Becker, K. H. *J. Atmos. Chem*. **1994**, *18*, 267.

(21) Chameides, W. L. *J. Geophys. Res*. **1984**, *89*, 4739.

(22) Matrozov, V. I.; Kashtanov, S. A.; Stepanov, A. M.; Tregubov, B. A. *Zh. Prikl. Khim*. **1976**, *49*, 1111.

(23) Miller, M. L.; Sheridan, C. L. *J. Phys. Chem*. **1956**, *60*, 184.

(24) Goldsack, D. E.; Franchetto, R. C. *Can. J. Chem*. **1978**, *56*, 1442.

(25) Sehested, K.; Corfitzen, H.; Holcman, J.; Hart, E. J. *J. Phys. Chem*. **1992**, *96*, 1005.

(26) Danckwerts, P. V. *Gas-Liquid Reactions*; McGraw-Hill Book Company: London, 1970.

(27) Kosak-Channing, L. F.; Helz, G. R. *Environ. Sci. Technol*. **1983**, *17*, 145.

(28) Schurath, U. *Labormessungen physikalisch-chemischer Parameter für die Modellierung des Stofftransports in Wolken- und Nebeltröpfchen*. Final report for EUROTRAC's subproject HALIPP, Bundesminster für Forschung und Technologie, FKZ 07EU727 9, 1994.

(29) Garland, J. A.; Elzerman, A. W.; Penkett, S. A. *J. Geophys. Res*. **1980**, *85*, 7488.

(30) Davies, D. M.; Deary, M. E. *J. Chem. Soc*. **1992**, *2*, 559.

(31) O'Sullivan, D. W.; Lee, M.; Noone, B. C.; Heikes, B. G. *J. Phys. Chem*. **1996**, *100*, 3241.

(32) De Bruyn, B. J.; Shorter, J. A.; Davidovits, P.; Worsnop, D. R.; Zahniser, M. S.; Kolb, C. E. *J. Geophys. Res*. **1992**, *99*, 16927.

(33) Jayne, J. T.; Davidovits, P.; Worsnop, D. R.; Zahniser, M. S.; Kolb, C. E. *J. Phys. Chem*. **1990**, *94*, 6041.

(34) Davidovits, P.; Jayne, J. T.; Duan, S. X.; Worsnop, D. R.; Zahniser, M. S.; Kolb, C. E. *J. Phys. Chem*. **1991**, *95*, 6337.

(35) Nathanson, G. M.; Davidovits, P.; Worsnop, D. R.; Kolb, C. E. *J. Phys. Chem*. **1996**, *100*, 13007.

(36) Schwartz, S. E. In *Chemistry of Multiphase Atmospheric Systems;* NATO ASI Ser. 4, Jaeschke, W., Ed.; Springer-Verlag: Berlin, 1986; p 415.